Inorganic Chemistry

Article

pubs.acs.org/IC

Thermal Decomposition Approach for the Formation of α-Fe_2O_3 Mesoporous Photoanodes and an α-Fe_2O_3/CoO Hybrid Structure for Enhanced Water Oxidation

Mahmud Diab and Taleb Mokari*

Department of Chemistry and Ilse Katz Center for Nanoscience and Nanotechnology, Ben-Gurion University of the Negev, 84105 Be'er Sheva, Israel

Supporting Information

ABSTRACT: Hematite (α-Fe_2O_3) is one of most investigated oxides for energy applications and specifically for photocatalysis. Many approaches are used to prepare well-controlled films of hematite with good photocatalytic performance. However, most of these methods suffer from a number of disadvantages, such as the small quantities of the product, and the assembly of the nanostructures is usually a secondary process. Herein, we present a facile and large-scale synthesis of mesoporous hematite structures directly on various substrates at moderate temperature and study their photoelectrochemical (PEC) properties. Our approach is based on thermal decomposition of iron acetate directly on a substrate followed by an annealing process in air to produce a continuous mesoporous film of α-Fe_2O_3, with good control of the size of the pores. Improving the PEC properties of iron oxide was achieved by deposition of CoO domains, which were formed by thermal decomposition of cobalt acetate directly onto the hematite surface to produce α-Fe_2O_3/CoO nanostructures. PEC measurements of the hematite film before and after CoO growth were tested. Two methods were used to deposit the cobalt material: (a) thermal decomposition and (b) the most typically used method, adsorption of cobalt salt. The photocurrent of pure hematite was 0.25 mA/cm^2 at 1.23 V versus reversible hydrogen electrode (RHE), while modification of the hematite surface using the thermal decomposition method showed 180% improvement (0.7 mA/cm^2 at 1.23 V vs RHE) and 40% improvement (0.35 mA/cm^2 at 1.23 V vs RHE) via the adsorption method. Moreover, the onset potential was shifted by 130 and 70 mV when the surface of the hematite was modified by the thermal decomposition and adsorption methods, respectively.

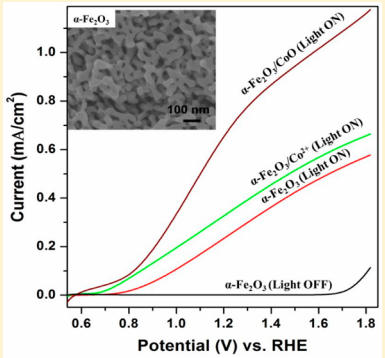

INTRODUCTION

Photoelectrochemical (PEC) water splitting uses a semiconductor material to absorb solar energy and create charges that is then used to split water molecules into hydrogen and oxygen.[1−3] In 1972, Fujishima and Honda were the first to report the usage of a semiconductor (TiO_2) in PEC cells.[2] Since then, extensive efforts have been aimed at finding a material that fulfills the necessary requirements of a good photocatalyst material for water splitting.[4−7] Metal oxides, such as TiO_2,[2] WO_3,[8] Cu_2O,[9] $BiVO_4$,[10] and α-Fe_2O_3, are good photocatalyst candidates for PEC water splitting because of their high stability in aqueous solutions and the alignment of their energy bands to the hydrogen and oxygen redox potentials. In addition, these materials are nontoxic, abundant, and simply fabricated.

α-Fe_2O_3 is one of the most promising materials for the photocatalytic process in PEC water splitting because of its further unique properties, such as its band gap (2.1 eV)[11] and theoretical maximum efficiency (12.9% AM 1.5).[12] However, hematite has low mobility ($<10^{-1}$ cm^2/V·s)[13] and a short diffusion length (<10 nm),[14] and the energetic position of the conduction band edge is low compared to the proton reduction potential. However, these limitations can be overcome by increasing the carrier populations through doping, increasing the size of the interface with the electrolyte, and controlling the shape of the material. These strategies, in combination with the use of an external electrical bias, enhance the performance of hematite in a PEC application.

In the past decade, several approaches were developed to synthesize hematite nanostructures with various morphologies, including solution-phase (hydrothermal,[15] solvothermal,[16] and sol−gel[17]), thermal oxidation,[18] pyrolysis,[19] electrochemical,[20] vapor-phase [metal−organic or atmospheric pressure chemical vapor deposition (MOCVD[21] or APCVD[22])], atomic layer deposition (ALD),[23] and sputtering techniques.[24] However, each method has its own disadvantages. For example, MOCVD and APCVD methods, which are typically conducted at high temperature, use flammable and toxic organic precursors. ALD and pyrolysis approaches need special apparatuses, and this, in turn, leads to an increase in the fabrication costs.[25] For the other techniques, the assembly of the nanocrystals onto a conducting electrode requires an additional process, and some devices formed through this method have poor PEC performance. Furthermore, in most of the approaches mentioned

Received: December 9, 2013
Published: January 28, 2014

   dx.doi.org/10.1021/ic403027r | Inorg. Chem. 2014, 53, 2304−2309

above, the hematite nanostructures are synthesized in small scales.

A mesoporous structure, with sufficient thickness, allows the material to absorb more light while keeping the distance between the electrolyte and hematite a few times its diffusion length. Some examples for this shape are silicon-doped cauliflower-type Fe_2O_3[22] and mesoporous hematite prepared by a colloidal method or directly grown on fluorine-doped tin oxide substrates.[26−28] Thus, by using this morphology, the probability of creating carriers that can reach the reactive surface is increased, and therefore the overall device efficiency is improved.

Coupling oxygen evolution reaction (OER) catalysts with these mesoporous structures enhances the performance of the water oxidation reaction by increasing the photocurrent and shifting the onset potential. For instance, interfacing IrO_2 (the best catalyst to date) with hematite resulted in a 200 mV shift in the photocurrent onset.[29] However, iridium is a rare and expensive material. Using low-cost materials, such as nickel oxide, cobalt ions Co^{II}, cobalt oxide (Co_3O_4), and cobalt phosphate (Co-Pi) resulted in 100, 80, 40, and 200 mV cathodic shifts, respectively.[22,30−34] This enhancement can be attributed either to the improvement of oxygen evolution kinetics or to the passivation of the surface or both. In most of the surface modifications mentioned above, the OER catalyst was prepared separately, before it was deposited onto the surface, except in the case of the Co_3O_4 catalyst, which was synthesized together with the hematite. Growth of the OER catalysts directly on the surface of the hematite has a direct impact on the PEC performance. We believe that the PEC performance of hematite can be further enhanced if the OER catalyst is formed on the surface because the quality of the interface between the catalyst and hematite can be improved as a result of the formation of direct contact between the catalyst and hematite.

Herein, we present a simple, safe, and general method to synthesize the mesoporous structure of α-Fe_2O_3 directly on a substrate on a large scale. This method is based on thermal decomposition of iron acetate [$Fe(ac)_2$] using organic solvents in a nitrogen atmosphere, which allows the synthesis and assembly of the nanocrystal at the same time. Moreover, we describe the formation of CoO through the thermal decomposition approach, directly onto the α-Fe_2O_3 surface. Then, we compare the PEC activity of the film after surface modification via the thermal decomposition approach and the Co^{2+} adsorption method.

EXPERIMENTAL SECTION

All solvents and reagents were purchased from Sigma-Aldrich or Strem Chemicals and used as received. Deionized (DI) water was purified using a Millipore Direct-Q system (18.2 MW·cm resistivity).

Structural Characterization. Scanning electron microscopy (SEM) was performed using a JEOL SM-7400F ultrahigh-resolution cold field-emission-gun SEM instrument operated at 3 kV and an energy-dispersive X-ray spectroscopy (EDX) detector. Phase analysis of the samples was done using the X-ray diffraction (XRD) method. The data were collected on a Philips 1050/70 diffractometer using Cu Kα radiation with a graphite monochromator on the diffracted beam and operated at 40 kV and 28 mA. UV−vis absorbance measurements were made using a Cary 5000 UV−vis−near-IR spectrophotometer. X-ray photoelectron spectroscopy (XPS) was performed using an ESCALAB 250 Thermo Fisher Scientific instrument.

PEC Measurements. PEC measurement of the hematite films was carried out in a 1 M KOH solution, using a VersaSTAT 3 potentiostat in a three-electrode system. The hematite film acts as the working electrode, a platinum wire as the counter electrode, and Ag/AgCl in saturated KCl as the reference electrode, separated by glass frits. The voltage was swept between −0.5 and +0.8 V vs Ag/AgCl at a scan rate 20 mV/s. The measured potential was converted to a reversible hydrogen electrode (RHE) using the Nernst equation. Light-emitting diodes (365 nm wavelength, ∼14 mW) were used as the light source to illuminate the substrate from the back side.

Synthesis of a Hematite Mesoporous Film. Iron acetate [$Fe(ac)_2$; 20 mg, 99.995%] was dissolved in trioctylphosphine oxide (TOPO; 0.3 mL, 99%) mixed with hexadecylamine (HDA; 0.6 mL, 90%) and 1-octadecene (0.3 mL, 90%). A droplet of this solution (30 μL) was deposited on a 0.8 × 2.5 cm^2 tin-doped indium oxide (ITO) substrate, which was cleaned using methanol, acetone, and isopropyl alcohol for 10 min by sonication in each solvent. The substrate was then heated on a hot plate under an inert atmosphere (inside a glovebox) for 15 min at 270 °C. A uniform layer of magnetite (Fe_3O_4) film (black color) was formed on the ITO substrate. Subsequently, the film was sintered in air at 400 °C for 5 h. During the sintering process, the nanoparticle film of magnetite was converted to a mesoporous film of hematite. For PEC measurements, samples were further annealed at 710 °C for 12 min.

Surface Modification of the Hematite Mesoporous Film. Surface modification of the hematite mesoporous film was attained by two approaches: (1) Decomposition of CoO where 3 mg of cobalt acetate [$Co(ac)_2$; 99.995%] was dissolved in 3 mL of TOPO (99%) mixed with 3 mL of HDA (90%). The solution (15 μL) was deposited on the hematite film. The substrate was then heated on a hot plate under an inert atmosphere (inside the glovebox) for 15 min at 270 °C. (2) Drop casting of $Co(NO_3)_2$ according to a previous report.[22] The hematite photoanode was briefly rinsed with DI water after PEC measurement and dried in a stream of air. The solution of $Co(NO_3)_2$ (10 mM) was deposited on the hematite surface (10 μL/cm^2). After a few seconds, the photoelectrode was rinsed again.

RESULTS AND DISCUSSION

Mesoporous Structure of the Hematite and Surface Modification. Hematite mesoporous films were synthesized on ITO substrates via thermal decomposition of $Fe(ac)_2$ followed by the annealing process (see the Experimental Section). When the sample was heated at 270 °C under an inert atmosphere, a uniform film of magnetite (Fe_3O_4) nanostructures was formed (Figure S1A in the Supporting Information, SI). Then, this film was sintered in air at 400 °C for 5 h (Figure S1B in the SI). During the sintering process, the film changes color from black to red, indicating a successful conversion from Fe_3O_4 to α-Fe_2O_3. Finally, the film was converted to a mesoporous structure. A SEM study of the surface of the film shows that the heating treatment increases the average size of the particle. Before annealing, the size of the Fe_3O_4 nanoparticles was found to be ∼12 nm (Figure S1A in the SI), and after conversion of the film from Fe_3O_4 to α-Fe_2O_3 at 400 °C, the average size of the particle increases to ∼25 nm (Figure S1B in the SI). Further sintering at 710 °C causes an additional increase to ∼45 nm (Figure 1A). A cross-sectional view of the film shows that the thickness of the film is ∼500 nm, as shown in Figure 1B. The XRD pattern obtained from this mesoporous film matches the diffraction pattern of the hematite bulk structure (Figure 1C). The absence of diffraction peaks of other phases of iron oxide confirms the complete conversion of Fe_3O_4 to α-Fe_2O_3.

Further verification of the structural conversion is obtained by the UV−vis absorption spectrum, as shown in Figure 1D. It shows a shoulder at ∼530 nm (2.34 eV) and a peak at ∼390 nm (3.18 eV), which are similar to the reported values in the literature.[35,36] The shoulder can be attributed to a spin-

dx.doi.org/10.1021/ic403027r | Inorg. Chem. 2014, 53, 2304−2309

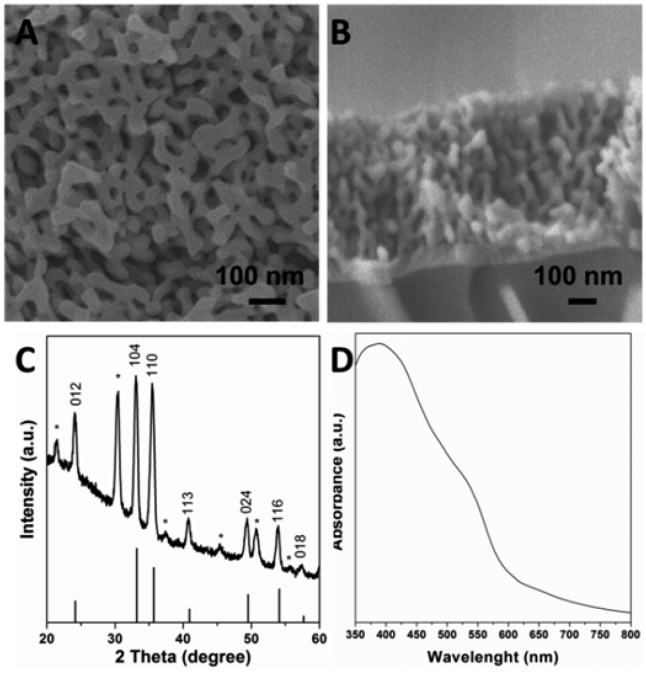

Figure 1. Structural characterization of iron oxide. (A and B) SEM images showing a top surface and cross-sectional view of the mesoporous film of α-Fe_2O_3, respectively. (C) XRD pattern of the hematite on the ITO substrate. Peaks marked with asterisks correspond to the ITO diffraction peaks. (D) Optical absorption spectrum of the hematite structure.

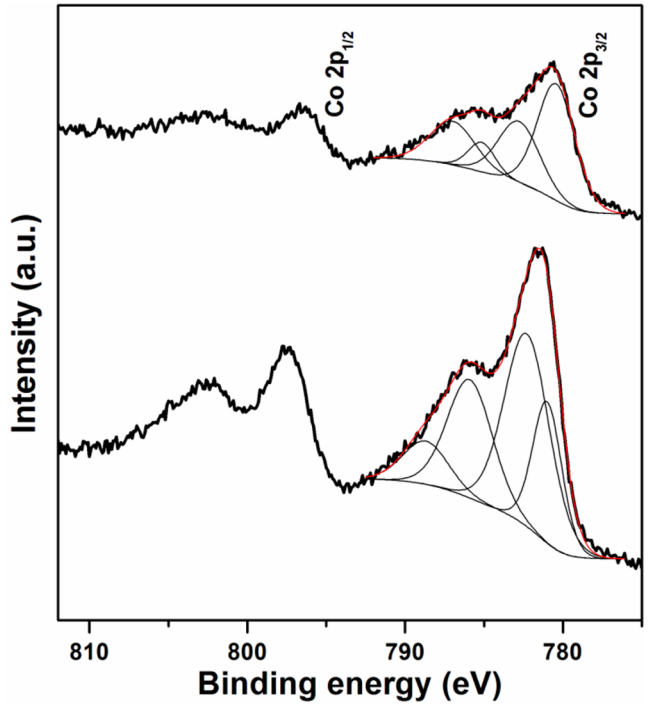

Figure 2. XPS spectra of the Co 2p scan. The upper trace corresponds to $Co(ac)_2$ after decomposition, and the bottom trace corresponds to $Co(ac)_2$.

forbidden Fe^{3+} 3d → 3d indirect transition, and the peak can be assigned to an O^{2-} 2p → Fe^{3+} 3d direct transition.[11]

As was mentioned before, the pure hematite material shows good catalytic activity. However, this activity can be improved by surface modification (cobalt deposition) via various approaches. In this report, we modify the surface of the α-Fe_2O_3 mesoporous film by deposition of a thin layer of cobalt monoxide (CoO) formed via thermal decomposition of a $Co(ac)_2$ solution directly on the hematite surface under nitrogen at 270 °C (see the Experimental Section).

Characterization of the Co_3O_4 product on the hematite surface was not possible by XRD and SEM. Therefore, more surface-sensitive techniques (EDX and XPS) were used to confirm the composition of Co_3O_4. XPS data reveal that decomposition of $Co(ac)_2$ on α-Fe_2O_3 did not show any change of the binding energy of the iron, as shown in Figure S2 in the SI. The binding energy of Fe $2p_{3/2}$ in both samples is positioned at ~710 eV (Figure S2 in the SI).[27,30] However, the XPS data for the Co 2p spectrum of $Co(ac)_2$ before and after decomposition show two main peaks in each spectrum, which can be assigned to Co $2p_{3/2}$ and Co $2p_{1/2}$, as shown in Figure 2. The differences in the peak positions between the two spectra prove that the binding energy of cobalt has changed, confirming a new composition for cobalt.

Previous works have reported that the binding energies of Co_3O_4 and cobalt hydroxides are similar in XPS spectra.[37−40] Therefore, it is not possible to distinguish between the various Co_3O_4 by examining only the main peaks, but looking for the presence or absence of additional spectral lines beside the main peaks can provide additional information about the composition. For example, satellite lines can be observed when the transition metals have unpaired electrons in the outer shell.[41] As we can see in Figure 2, the appearance of the satellite peaks beside the main peaks indicates that the product of decomposition does not contain Co^{3+} but mainly Co^{2+}, which can be either CoO or $Co(OH)_2$.[42] Furthermore, in our previous work,[43] we found that thermal decomposition of 40 mg of $Co(ac)_2$ in a mixture of TOPO and HDA (similar to the conditions used here) produces CoO. Thus, we assume that we have formed CoO and not $Co(OH)_2$. Moreover, decomposition of the cobalt salt on the hematite did not change the crystal structure of the hematite, as shown in Figure S3 in the SI.

To examine coverage of Co_3O_4 on the hematite surface, elemental mapping of Fe, O, and Co was performed using EDX analysis over a large area of the sample. Figure S4 in the SI presents the EDX data, which show good coverage of the cobalt. The effect of the coverage and concentration of $Co(ac)_2$ on the PEC performance of the hematite will be discussed later.

PEC Performance. Initially, the hematite photoanode was further annealed for 12 min at 710 °C to achieve better performance. Previous reports have shown that annealing the hematite on the ITO substrate at high temperatures leads to diffusion of Sn atoms from the substrate into the hematite, which improves its conductivity[26,44] or simply improves the crystallinity of the hematite and the electrical contact with the substrate.[45] We tested the PEC performance of the hematite photoanode without activation at 710 °C and observed a negligible PEC performance, as shown in Figure S5 in the SI.

The PEC measurements of the hematite mesoporous film before and after surface modification are shown in Figure 3. Pure hematite mesoporous films scanned in the dark (Figure 3, black line) show a maximum current of 0.11 mA/cm^2 at 1.82 V vs RHE with an onset potential of ~1.6 V vs RHE. However, upon irradiation (Figure 3, red line), the mesoporous photoanode shows a maximum photocurrent of 0.58 mA/cm^2 at 1.82 V vs RHE with an onset potential of ~0.71 V vs RHE.

dx.doi.org/10.1021/ic403027r | Inorg. Chem. 2014, 53, 2304−2309

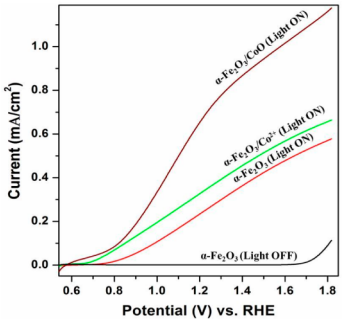

Figure 3. Photocurrent potential versus voltage scans for the hematite film before and after surface modification, with a scan rate of 20 mV/s: hematite without modification in the dark (black line) and in light (red line); hematite with a $Co(NO_3)_2$ overlayer (green line); hematite with a CoO overlayer (brown line).

This potential onset is relatively low compared to other values observed with a hematite photoanode without surface modification.[11,26,46] Different ways to reduce the onset potential of the water oxidation were reported in the literature, either by passivation of surface recombination sites, improving the kinetic of OER,[4,47−50] or by forming a p−n junction structure, which enhances the separation of the charges.[30,51,52] Herein, we tested the reduction of the onset potential by modifying the hematite surface in two methods: thermal decomposition of $Co(ac)_2$ directly on the hematite surface to produce CoO and drop casting of the $Co(NO_3)_2$ method, which is the most commonly used approach in the literature (Experimental Section). Both treatments lead to a cathodic shift of the onset potential of water oxidation. CoO modification (Figure 3, brown line) shows a ∼130 mV shift and a maximum photocurrent of 1.17 mA/cm^2 at 1.82 V vs RHE. However, there is a 70 mV shift and a maximum photocurrent of 0.66 mA/cm^2 at 1.82 V vs RHE when $Co(NO_3)_2$ modification is used (Figure 3, green line). The electrode with $Co(NO_3)_2$ modification has been optimized by running multiple cycles to give the maximum current (Figure S6 in the SI). This difference in the enhancement of the PEC performance can be explained by passivation of the surface sites and an increase of the hole lifetime.

It is known that Co^{2+} modification cannot passivate the surface traps;[53] however, they can be passivated by a Co_3O_4 overlayer.[54] Furthermore, it was observed that the lifetime of the hole is significantly increased when Co_3O_4 is used for surface modification.[54] We further believe that thermal decomposition of cobalt salt directly onto the hematite surface can potentially have an additional contribution to the enhancement because during the decomposition process, CoO can form a direct contact with the α-Fe_2O_3 surface, which facilitates transport of the holes and also provides better passivation of the surface traps. For these reasons, we obtained 100% improvement of the PEC performance at 1.82 V vs RHE when the thermal decomposition method is used, compared to 15% improvement using the adsorption approach.

To study the stability of the hematite before and after surface treatments, a fixed voltage (1.23 V vs RHE) was applied on the samples, and the photocurrent was measured as a function of time via on−off cycles of irradiation. As shown in Figure 4, all of the samples show high stability, and the photocurrents decrease less than 3% in the case of hematite and less than 1% upon modification with CoO and $Co(NO_3)_2$, after a total of 7.5 min. However, the transient photocurrent of CoO−hematite

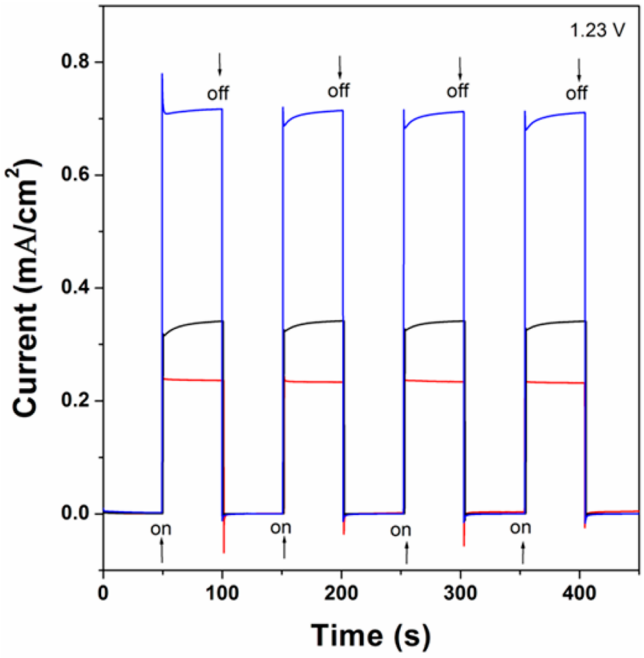

Figure 4. Photocurrent potential versus time scans for the hematite film before and after surface modification, with 1.23 V vs RHE: pure hematite (red); hematite with a $Co(NO_3)_2$ overlayer (black); hematite with a CoO overlayer (blue).

modification is higher than 0.7 mA/cm^2 at 1.23 V vs RHE, whereas those of $Co(NO_3)_2$−hematite modification and pure hematite are 0.35 and 0.25 mA/cm^2 at 1.23 V vs RHE, respectively.

To further understand the effect of CoO on the hematite performance, different amounts of $Co(ac)_2$ were thermally decomposed on the hematite surface. The experiment was carried out by adding a series of different amounts of a $Co(ac)_2$ stock solution [0.5 mg/mL $Co(ac)_2$ in a mixture of TOPO and HDA]. The photocurrent for all electrodes was measured versus the applied voltage, as presented in Figure 5. The photocurrent increases as the cobalt salt amount increases until it reaches 15 μL. A further increase in the cobalt salt amount reduces the photocurrent. This trend is illustrated clearly in the inset of Figure 5, where the current was plotted versus the amount of $Co(ac)_2$ solution at 1.23 V (vs RHE). Furthermore, we did not observe any change in the potential onset. The increase of the current while increasing the amount of cobalt salt to 15 μL can be attributed to passivation of the surface traps and also to the possibility of forming a hole acceptor on the hematite surface, which can improve the kinetics of the OER. However, a further increase in the amount of cobalt salt leads to aggregation of the Co_3O_4 nanoclusters into larger Co_3O_4 particles, which decreases the contact of the catalyst with the hematite surface and decreases the absorption efficiency of the hematite.

■ CONCLUSIONS

The mesoporous structure of α-Fe_2O_3 is synthesized by a simple, safe, and general method with the capability for scale-up. This approach is based on two steps: first thermal decomposition of $Fe(ac)_2$ directly onto the ITO substrate at moderate temperature in a nitrogen atmosphere followed by a sintering process in air at high temperature. We found that the average size of the nanoparticles can be altered by the

dx.doi.org/10.1021/ic403027r | Inorg. Chem. 2014, 53, 2304−2309

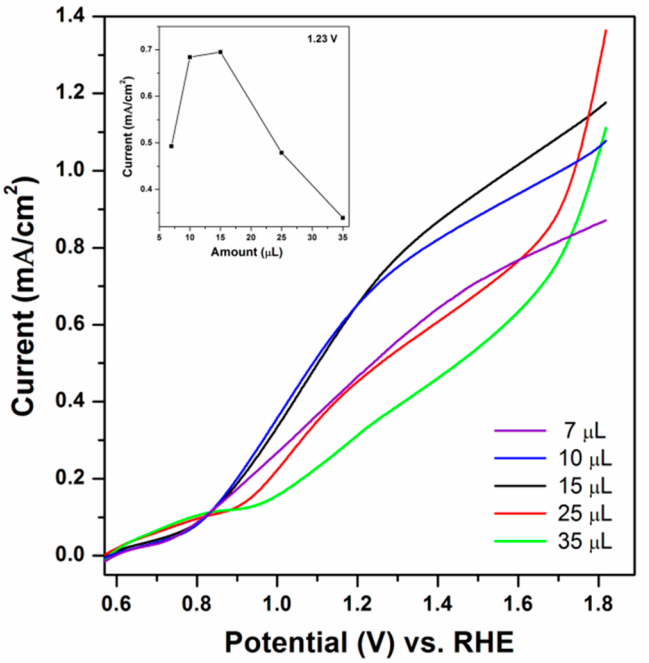

Figure 5. Thermal decomposition of various amounts of $Co(ac)_2$ in a mixture of TOPO and HDA on the surface of the hematite and their effect on the performance of the electrode: 7 μL, purple line; 10 μL, blue line; 15 μL, black line; 25 μL, red line; 35 μL, green line. Inset: current versus amount of $Co(ac)_2$ solution at 1.23 V vs RHE.

temperature: 25 and 45 nm when the annealing process is conducted at 400 and 710 °C, respectively. We show that the PEC performance of the hematite structures can be improved by surface passivation and catalyst deposition. Thermal decomposition of the $Co(ac)_2$ salt to form CoO nanostructures was found to enhance the PEC activity of the hematite film better than deposition of the $Co(NO_3)_2$ salt.

■ ASSOCIATED CONTENT

Ⓢ Supporting Information

SEM images for iron oxide before and after the annealing process, EDX and XPS data, XRD pattern, and current−voltage curves. This material is available free of charge via the Internet at http://pubs.acs.org.

■ AUTHOR INFORMATION

Corresponding Author

*E-mail: mokari@bgu.ac.il.

Author Contributions

The manuscript was written through contributions of all authors. All authors have given approval to the final version of the manuscript.

Notes

The authors declare no competing financial interest.

■ ACKNOWLEDGMENTS

This work was supported by the European Research Council (starting grant, Project 278779) and partially supported by the I-CORE Program of the Planning and Budgeting Committee and the Israel Science Foundation (Grant 152/11). M.D. thanks the Fohs Foundation Undergraduate and Graduate Scholarship Fund. The authors thank Dr. Natalya Froumin for XPS measurements and Dmitry Mogilyansky for XRD measurements.

■ REFERENCES

(1) Khaselev, O.; Turner, J. A. *Science* **1998**, *280*, 425−427.
(2) Fujishima, A.; Honda, K. *Nature* **1972**, *238*, 37−38.
(3) Grätzel, M. *Nature* **2001**, *414*, 338−344.
(4) Sivula, K.; Le Formal, F.; Grätzel, M. *ChemSusChem* **2011**, *4*, 432−449.
(5) Currao, A. *Chimia* **2007**, *61*, 815−819.
(6) Walter, M. G.; Warren, E. L.; McKone, J. R.; Boettcher, S. W.; Mi, Q.; Santori, E. A.; Lewis, N. S. *Chem. Rev.* **2010**, *110*, 6446−6473.
(7) Kudo, A.; Miseki, Y. *Chem. Soc. Rev.* **2009**, *38*, 253−278.
(8) Abe, R.; Takata, T.; Sugihara, H.; Domen, K. *Chem. Commun.* **2005**, *30*, 3829−3831.
(9) Paracchino, A. *Nat. Mater.* **2011**, *10*, 456−461.
(10) Hou, Y.; Zuo, F.; Dagg, A.; Feng, P. *Nano Lett.* **2012**, *12*, 6464−6473.
(11) Duret, A.; Grätzel, M. *J. Phys. Chem. B* **2005**, *109*, 17184−17191.
(12) Murphy, A.; Barnes, P.; Randeniya, L.; Plumb, I.; Grey, I.; Horne, M.; Glasscock, J. *Int. J. Hydrogen Energy* **2006**, *31*, 1999−2017.
(13) Gardner, R. F. G.; Sweett, F.; Tanner, D. W. *J. Phys. Chem. Solids* **1963**, *24*, 1183−1196.
(14) Kennedy, J. H. *J. Electrochem. Soc.* **1978**, *125*, 709−714.
(15) Li, Z.; Lai, X.; Wang, H.; Mao, D.; Xing, C.; Wang, D. *Nanotechnology* **2009**, *20*, 245603−245612.
(16) Kim, H.-J.; Choi, K.-I.; Pan, A.; Kim, I.-D.; Kim, H.-R.; Kim, K.-M.; Na, C. W.; Cao, G.; Lee, J.-H. *J. Mater. Chem.* **2011**, *21*, 6549−6555.
(17) Woo, K.; Lee, H. J.; Ahn, J.-P.; Park, Y. S. *Adv. Mater.* **2003**, *15*, 1761−1764.
(18) Rao, P. M.; Zheng, X. L. *Nano Lett.* **2009**, *9*, 3001−3006.
(19) Mooney, J. B.; Radding, S. B. *Annu. Rev. Mater. Sci.* **1982**, *12*, 81−101.
(20) LaTempa, T. J.; Feng, X. J.; Paulose, M.; Grimes, C. A. *J. Phys. Chem. C* **2009**, *113*, 16293−16298.
(21) Wu, J. J.; Lee, Y. L.; Chiang, H. H.; Wong, D. K. P. *J. Phys. Chem. B* **2006**, *110*, 18108−18111.
(22) Kay, A.; Cesar, I.; Grätzel, M. *J. Am. Chem. Soc.* **2006**, *128*, 15714−15721.
(23) Lin, Y.; Zhou, S.; Sheehan, S. W.; Wang, D. *J. Am. Chem. Soc.* **2011**, *133*, 2398−2401.
(24) Hahn, N. T.; Ye, H. C.; Flaherty, D. W.; Bard, A. J.; Mullins, C. B. *ACS Nano* **2010**, *4*, 1977−1986.
(25) Wheeler, D. A.; Wang, G.; Ling, Y.; Li, Y.; Zhang, J. Z. *Energy Environ. Sci.* **2012**, *5*, 6682−6702.
(26) Sivula, K.; Zboril, R.; Le Formal, F.; Robert, R.; Weidenkaff, A.; Tucek, J.; Frydrych, J.; Grätzel, M. *J. Am. Chem. Soc.* **2010**, *132*, 7436−7444.
(27) Wang, G.; Ling, Y.; Wheeler, D.; George, K. E. N.; Horsley, K.; Heske, C.; Zhang, J. Z.; Li, Y. *Nano Lett.* **2011**, *11*, 3503−3509.
(28) Brillet, J.; Grätzel, M.; Sivula, K. *Nano Lett.* **2010**, *10*, 4155−4160.
(29) Tilley, S. D.; Cornuz, M.; Sivula, K.; Grätzel, M. *Angew. Chem., Int. Ed.* **2010**, *49*, 6405−6408.
(30) Li, J.; Meng, F.; Suri, S.; Ding, W.; Huang, F.; Wu, N. *Chem. Commun.* **2012**, *48*, 8213−8215.
(31) Xi, L.; Tran, P. D.; Chiam, S. Y.; Bassi, P. S.; Mak, W. F.; Mulmudi, H. K.; Batabyal, S. K.; Barber, J.; Loo, J. S. C.; Wong, L. H. *J. Phys. Chem. C* **2012**, *116*, 13884−13889.
(32) Klahr, B.; Gimenez, S.; Fabregat-Santiago, F.; Bisquert, J.; Hamann, T. W. *J. Am. Chem. Soc.* **2012**, *134*, 16693−16700.
(33) Barroso, M.; Cowan, A. J.; Pendlebury, S. R.; Grätzel, M.; Klug, D. R.; Durrant, J. R. *J. Am. Chem. Soc.* **2011**, *133*, 14868−14871.
(34) Zhong, D. K.; Cornuz, M.; Sivula, K.; Grätzel, M.; Gamelin, D. R. *Energy Environ. Sci.* **2011**, *4*, 1759−1764.
(35) Marusak, L. A.; Messier, R.; White, W. B. *J. Phys. Chem. Solids* **1980**, *41*, 981−984.

(36) Debnath, N. C. *J. Electrochem. Soc.* **1982**, *129*, 2169−2174.
(37) Biesinger, M. C.; Payne, B. P.; Grosvenor, A. P.; Lau, L. W. M.; Gerson, A. R.; Smart, R. S. C. *Appl. Surf. Sci.* **2011**, *257*, 2717−2730.
(38) Yang, J.; Liu, H.; Martens, W. N.; Frost, R. L. *J. Phys. Chem. C* **2010**, *114*, 111−119.
(39) Barreca, D.; Massignan, C.; Daolio, S.; Fabrizio, M.; Piccirillo, C.; Armelao, L.; Tondello, E. *Chem. Mater.* **2001**, *13*, 588−593.
(40) Shi, R.; Chen, G.; Ma, W.; Zhang, D.; Qiu, G.; Liu, X. *Dalton Trans.* **2012**, *41*, 5981−5987.
(41) Mekki, A.; Holland, D.; Ziq, K.; Mcconville, C. F. *J. Non-Cryst. Solids* **1997**, *3*, 267−279.
(42) Riha, S. C.; Klahr, B. M.; Tyo, E. C.; Seifert, S.; Vajda, S.; Pellin, M. J.; Hamann, T. W.; Martinson, A. B. F. *ACS Nano* **2013**, *7*, 2396−2405.
(43) Diab, M.; Volokh, M.; Moshofsky, B.; Jen-La Plante, I.; Flomin, K.; Chockler, E.; Mokari, T. *Isr. J. Chem.* **2012**, *52*, 1081−1089.
(44) Ling, Y.; Wang, G.; Wheeler, D.; Zhang, J. Z.; Li, Y. *Nano Lett.* **2011**, *11*, 2119−2125.
(45) Li, L.; Yu, Y.; Meng, F.; Tan, Y.; Hamers, R. J.; Jin, S. *Nano Lett.* **2012**, *12*, 724−731.
(46) Hahn, N. T.; Mullins, C. B. *Chem. Mater.* **2010**, *22*, 6474−6482.
(47) Hisatomi, T.; Le Formal, F.; Cornuz, M.; Brillet, J.; Tétreault, N.; Sivula, K.; Grätzel, M. *Energy Environ. Sci.* **2011**, *4*, 2512−2515.
(48) Seabold, J. A.; Choi, K. *Chem. Mater.* **2011**, *23*, 1105−1112.
(49) Spray, R. L.; McDonald, K. J.; Choi, K. *J. Phys. Chem. C* **2011**, *115*, 3497−3506.
(50) Zhong, D. K.; Gamelin, D. R. *J. Am. Chem. Soc.* **2010**, *132*, 4202−4207.
(51) Lin, Y.; Xu, Y.; Mayer, M. T.; Simpson, Z. I.; McMahon, G.; Zhou, S.; Wang, D. *J. Am. Chem. Soc.* **2012**, *134*, 5508−5511.
(52) McDonald, K. J.; Choi, K. *Chem. Mater.* **2011**, *23*, 4863−4869.
(53) Le Formal, F.; Tétreault, N.; Cornuz, M.; Moehl, T.; Grätzel, M.; Sivula, K. *Chem. Sci.* **2011**, *2*, 737−743.
(54) Barroso, M.; Mesa, C. A.; Pendlebury, S. R.; Cowan, A. J.; Hisatomi, T.; Sivula, K.; Grätzel, M.; Klug, D. R.; Durrant, J. R. *Proc. Natl. Acad. Sci. U.S.A.* **2012**, *109*, 15640−15645.